Title

Comparison of tibiofemoral joint space width measurements from standing CT and fixed flexion radiography

Journal

Journal of Orthopaedic Research®, 35(7)

ISSN

0736-0266

Authors

Segal, Neil A
Frick, Eric
Duryea, Jeffrey
et al.

Publication Date

2017-07-01

DOI

10.1002/jor.23387

Peer reviewed

HHS Public Access

Author manuscript

J Orthop Res. Author manuscript; available in PMC 2018 July 01.

Published in final edited form as:

J Orthop Res. 2017 July ; 35(7): 1388–1395. doi:10.1002/jor.23387.

Comparison of Tibiofemoral Joint Space Width Measurements from Standing CT and Fixed Flexion Radiography

Neil A. Segal[1,2], **Eric Frick**[3], **Jeffrey Duryea**[4], **Michael C. Nevitt**[5], **Jingbo Niu**[6], **James C. Torner**[2], **David T. Felson**[6], and **Donald D. Anderson**[3]

[1]Department of Rehabilitation, The University of Kansas (Kansas City, KS)

[2]Department of Epidemiology, The University of Iowa College of Public Health (Iowa City, IA)

[3]Department of Orthopaedics & Rehabilitation, The University of Iowa (Iowa City, IA)

[4]Brigham and Women's Hospital/Harvard Medical School (Boston, MA, USA)

[5]Department of Epidemiology & Biostatistics, University of California, San Francisco (San Francisco, CA)

[6]Clinical Epidemiology Research & Training Unit, Boston University School of Medicine (Boston, MA)

Abstract

The objective of this project was to determine the relationship between medial tibiofemoral joint space width measured on fixed-flexion radiographs and the three-dimensional joint space width distribution ona low-dose, standing CT (SCT) imaging. At the 84-month visit of the Multicenter Osteoarthritis Study, 20 participants were recruited. A commercial SCT scanner for the foot and ankle was modified to image knees while standing. Medial tibiofemoral joint space width was assessed on radiographs at fixed locations from 15–30% of compartment width using validated software and on SCT by mapping the distances between three-dimensional subchondral bone surfaces. Individual joint space width values from radiographs were compared with three-dimensional joint space width values from corresponding sagittal plane locations using paired t-tests and correlation coefficients. For the 4 medial-most tibiofemoral locations, radiographic joint space width values exceeded the minimal joint space width on SCT by a mean of 2.0mm and were approximately equal to the 61st percentile value of the joint space width distribution at each respective sagittal-plane location. Correlation coefficients at these locations were 0.91–0.97 and the offsets between joint space width values from radiographs and SCT measurements were

Corresponding Author: Dr. Neil A. Segal, The University of Kansas, Department of Rehabilitation Medicine, 3901 Rainbow Boulevard, Mailstop 1046, Kansas City, KS 66160, FAX: (913) 588-6765, segal-research@uiowa.edu.

Author contributions: Responsibility for the integrity of the work as a whole: N. A. Segal
Study concept and design: N. A. Segal, D. D. Anderson, M. C. Nevitt
Acquisition of data: N. A. Segal, J. Duryea
Analysis and interpretation of data: J. Niu, N. A. Segal, D. D. Anderson, E. Frick, D. T. Felson
Drafting of the manuscript: N. A. Segal, D. D. Anderson, E. Frick, J. Niu, M. C. Nevitt
Critical revision of the manuscript for important intellectual content: all authors
Statistical Expertise: J. Niu
Obtained funding: N. A. Segal
Administrative, technical, or material support: J. C. Torner, M. C. Nevitt, D. T. Felson
All authors have read and approved the final submitted manuscript.

consistent. There were greater offsets and variability in the offsets between modalities closer to the tibial spine. Joint space width measurements on fixed-flexion radiographs are highly correlated with three-dimensional joint space width from SCT. In addition to avoiding bony overlap obscuring the joint, a limitation of radiographs, the current study supports a role for SCT in the evaluation of tibiofemoral OA.

Keywords

joint space width; osteoarthritis; imaging; knee; cartilage loss

Introduction

Osteoarthritis (OA) is the most prevalent musculoskeletal disease in US adults, and the knee is the most commonly affected weight-bearing joint.[1] Despite its high prevalence, knee OA is not readily diagnosed in a manner that allows providers to institute preventive therapies or to assess the outcomes of therapies.

Radiographic abnormalities have demonstrated poor agreement with both arthroscopy and MRI findings in a number of studies.[2-5] Some of the reasons for these poor correlations with joint structure may include: 1) the two-dimensional (2D) nature of radiographs limiting visualization of joint structures, 2) poor reproducibility of the joint space imaging angle, 3) inability to account for either cartilage or menisci. These limitations of radiographs make them poorly suited for detecting a disease that affects the whole joint (bone, cartilage, menisci, synovium, ligaments, muscles), as well as for measuring a dynamic disease with subtle changes over time that occur in only a subset of patients.

Due to radiographs evaluating a 3D structure as a 2D projection, variability in joint positioning has a large impact on appearance of the joint space. The resulting error causes substantial imprecision in measurements of joint space width (JSW), the distance between the projected femoral and tibial margins on radiographic images.[5] According to one study, over half of knees without radiographic evidence of OA had at least partial-thickness cartilage loss.[6] In addition, on direct visualization with arthroscopy, many knees graded as “completely normal” based on radiographs have severe OA (false negatives), and those with apparent tibiofemoral JSW loss frequently have normal articular cartilage (false positives).[2] Studies have demonstrated that, in knees at elevated risk for OA, radiographs frequently fail to capture changes in JSW over 4 years of follow-up.[4; 5; 7; 8] These inherent limitations can restrict the ability of OA clinical trials to detect efficacy of new therapies within the usual 1–2 year time frame and also prevent clinicians from detecting knee OA changes until joint damage is advanced.[5; 9] Despite these challenges, JSW on weight-bearing radiographs is the only structural outcome approved for Phase III trials by the FDA[10] or the European Medicines Agency.[11]

Given the poor sensitivity of the standard diagnostic test for knee OA, a highly prevalent disease with a severe functional impact, there is a compelling need for a more sensitive imaging biomarker. A more ideal imaging biomarker for monitoring joint structure would provide higher sensitivity and accuracy without significantly increasing the radiation dose,

time or cost. Digital x-ray tomosynthesis (DTS) has been proposed as a means to improve accuracy of JSW measurements over those available from plain radiographs.[12; 13] While DTS has demonstrated sub-millimeter accuracy, JSW measurements are represented 2-dimensionally and limitations include image acquisition over a limited angular range of 20-60°, anisotropic resolution, tomosynthesis artifacts, limited soft-tissue visualization, and the need for specialized tomosynthesis acquisition and post-processing.

Low dose CT acquired while standing (SCT) may address these limitations through 360° image acquisition that provides isotropic visualization and 3D JSW map of the tibiofemoral as well as patellofemoral joints, while also providing visualization of the menisci. If SCT were to enhance validity of JSW measurements, through improved visualization of structural effects of knee OA, the cost and duration of OA clinical trials may be reduced, accelerating scientific progress and advancing clinical care. A potential additional advantage of SCT would be the ability to obtain a 3D representation of the knee joint in a weight-bearing configuration, permitting detection of abnormal contact stress patterns, which may be predictive of future disease worsening[14; 15].

As an initial step in evaluating SCT for assessment of knee joint space width, we compared JSW measurements made at fixed locations ($JSW_{(x)}$) on fixed-flexed radiographs—a flawed, but widely-used imaging method— with the anteroposterior distribution of 3D JSW at corresponding sagittal-plane locations on SCT imaging, with the aim of assessing the correlation and offset between the accepted standard, radiographic $JSW_{(x)}$, and 3D JSW measurements on SCT.

Methods

Subjects

This study was conducted ancillary to the 84-month visit of the Multicenter Osteoarthritis Study (MOST), an NIH-funded longitudinal observational study of 3026 community-dwelling men and women, who at baseline were age 50-79 with knee OA or with known risk factors for knee OA. Enrollment for MOST has been described previously[16].Participants in the present study were a convenience sample of those at the University of Iowa site who had bilateral knee radiographs in the prior 6 months, met MOST reading center quality control criteria, had bilateral Kellgren Lawrence[17] (KL) grade <4, had knees discordant for KL grade (in order to represent a range of OA features and severity), who lived in proximity to our clinical center and whose distal thigh width measured on PA radiographs did not exceed the 38.1cm SCT gantry width. Out of 83 MOST participants who met inclusion criteria, the first 20 who volunteered were recruited. An enrollment flow-chart is presented in Figure 1. All participants completed an institutional review board-approved informed consent process.

Image Acquisition and JSW measurements

At the 84-month MOST clinic visit, bilateral, standing fixed-flexion posteroanterior (PA) radiographs of the tibiofemoral compartments were acquired using a plexiglass positioning frame (SynaFlexer; Synarc, Inc, San Francisco, California, USA).[19] The right and left knees were imaged at 70 kVp, together on 35.6×43.2cm CR plate with a 72-inch film-to-focus

distance, at a pixel size of 0.2mm using Fuji FCR Carbon X (v6.0) CR Equipment. The cranio-caudal beam angle was between 5° and 15°, selected for each participant at baseline to give a level medial tibial plateau (Further details available at http://www.most.ucsf.edu).Following acquisition, radiographs were graded according to the KL grading system, with disagreements adjudicated by consensus reading.[17; 18]

Radiographic JSW between the projected femoral and tibial bone margins is the currently accepted metric for longitudinal assessment of knee OA disease status. Duryea et al. developed and documented a semi-automated software tool,[20; 21] to delineate the femoral and tibial margins on digitized knee radiographs and enable measurements of JSW at seven fixed locations within the medial tibiofemoral compartment ($JSW_{(x)}$). In brief, this method involves establishment of a coordinate system referenced to anatomical landmarks (Figure 2a). The software automatically calculated the x-axis, defined as the line tangent to both femoral epicondyles. Thus, each x-location represented the position of the $JSW_{(x)}$ measurement along the projected tibiofemoral joint. The y-axis (x=0), a line perpendicular to the x-axis and tangent to the greatest prominence of the medial femoral epicondyle was placed manually. The line x=1, was defined as the tangent to the greatest prominence of the lateral femoral epicondyle. The variable x is thus a dimensionless quantity that represents the fractional distance from the most medial to the most lateral extents of the tibiofemoral joint. Prior studies established the reproducibility of this technique.[21] and explored the responsiveness for each of these over time in knees of varying OA severity.[22]

For SCT, a commercial scanner (PedCAT, Curvebeam LLC, Warrington, PA) was modified to enable imaging of bilateral knees while standing in the same fixed-flexed position used for the radiograph protocol. A custom radiolucent positioning device was used to maintain foot external rotation and fixed knee flexion angles equivalent to those used for the fixed-flexion radiographs (Figure 3), with patellae and thighs against a surface coplanar with the anterior extent of their toes, their pelvis centered above their feet and their torso and head vertical, looking straight ahead at a point at eye level. Participants' feet, knees, thighs, forearms and hands remained in contact with the device for stability and minimization of motion.

The scanner produced pulsed cone-beam x-ray on a 30 × 30 cm amorphous silicon flat-panel detector, over a 360° projection angle. The detector was used in 2×2 binning mode with 388μm effective pixel size measured at the detector plane. A 3D dataset with isotropic resolution of 0.37 mm and field of view of 200×350 mm was reconstructed from initial cone-beam projections. Reconstructed images were uploaded to a PACS as a standard DICOM CT image stack with image matrix of 950×950×533 pixels and 0.37 mm slice thickness. The University of Iowa Environmental Health and Safety Health Physics Associate performed a radiation survey of the CurveBeam SCT. Scatter measurements were made using a calibrated Unfors Xi model 9000 (Unfors RaySafe, Inc., Cleveland, OH) with a survey detector for scatter measurements and a CT detector for direct beam measurements. Background x-ray radiation was 0.00001 mSv/hr. Air kerma values measured at the entrance (skin) plane were as follows: at knee level, 1.2mGy; 10cm above the knee, 0.06 mGy; at a 1m distance, 0.0031 mGy; and at a 3m distance, 0.0003 mGy. The effective dose was

calculated by multiplying the air kerma value by the appropriate tissue weighting factor for skin and bone. The effective dose at knee level was 0.024 mSv.

Three-dimensional analysis of the SCT DICOM files required several steps; the first of which was segmentation. Using custom MatLab code, the DICOM files were separated into bone and non-bone portions using a series of thresholding algorithms utilizing the higher density of bone as compared with the surrounding soft tissues. Due to the thinness of the denser cortical bone in methaphyseal areas, the resulting segmentation masks were manually reviewed and edited as needed to ensure the accuracy of the segmented bone models. The non-bone portions, as well as the patella and fibula, were then removed leaving only the triangulated surfaces of the femur and tibia. Once segmentation was complete, the subchondral surfaces of the femur and tibia were isolated. The tesellated surfaces from the raw segmentations were lightly smoothed using Geomagic Studio software (Geomagic, Inc., Research Triangle Park, NC). Surface features were smoothed judiciously, balancing a desire for smoothness with the need to preserve local surface irregularities. In prior work using a similar approach in the ankle, the average 3D deviation between raw and smoothed surfaces was 0.32 mm.[23] In another study in which an identical smoothing approach was physically validated, the excellent agreement found between computationally predicted and physically measured contact stress supported that the bones were accurately segmented.[24]

The subchondral bone surfaces were then used to find the nearest-neighboring element of the femur for each element on the tibia, resulting in every element on the tibial subchondral bone surface being assigned a distance to the femoral subchondral surface. The distances were color-coded and overlaid on the tibial articular surface to visually display the data, producing a map of the 3D JSW at every point on the subchondral surface (Figure 4). These color-coded maps were then resolved into distance-area data. The area of each element on the tibial surface was calculated and paired with the previously calculated distance, resulting in a two-column matrix of distance-area pairs. A maximum distance of 10mm was selected to define the contacting regions of the joint, and the surface area of every element with a distance ≤10mm was summed to generate the total tibial subchondral area.

In order to compare the 3D SCT data with the same mediolateral x-locations at which the 2D data from$JSW_{(x)}$ measurements were made on fixed-flexion radiographs (Figure 2b), the coordinate systems were closely matched, by first matching the 3D SCT configuration to the coronal radiographic projection to co-register the x and y axes. This was achieved in an analogous manner as was used for finding the locations on radiographs. The most medial extent of the medial femoral epicondyle was defined as x=0 and the most lateral extent of the lateral femoral epicondyle was defined as x=1. The z-axis defined the anteroposterior locations at each x-location (.15, .175, .2, .225, .25, .275, and .3). The z-values from the posterior edge to the anterior edge of the tibial articular surface were found via interpolation of the previously calculated distance data (Figure 4). This resulted in measurements of JSW at approximately 250 z-value locations for each x-location. The reproducibility of medial compartment JSW measurements on 50 knee scans acquired 2 weeks apart had a test-retest reliability $ICC_{2,1}$ of 0.97 (95%CI: 0.94–1.00).

Statistical Methods

As the coordinate frame from the $JSW_{(x)}$ measurements on fixed flexion radiographs was copied to the 3D SCT images, direct comparisons were made between radiographic $JSW_{(x)}$ and the anteroposterior distribution of JSW at each of the seven x-values on SCT. Due to the need to compare each single $JSW_{(x)}$ with the approximately 250 measurements of JSW along an anteroposterior line at that x-location on the 3D surface, the SCT JSW data were summarized by calculating percentile distributions of the JSW values at each of the 7 mediolateral x-locations. To avoid the potential for the 0^{th} percentile representing an outlier value and to compare with the range close to the radiographic JSWx values, the 20^{th} percentile and 60^{th} percentile of the 3D JSW distribution at each x-location were used for comparison with each corresponding radiographic $JSW_{(x)}$ value. Pearson correlations coefficients were calculated for the $JSW_{(x)}$ vs. each percentile distribution and bootstrapping was used to calculate 95% CI for the correlation coefficients. Paired t-tests were used to assess the mean differences between the radiographic and SCT measurements at each x-location and also to find the regions of equivalency between the measurements. Finally, the mean $JSW_{(x)}$ data were overlaid on the distribution of JSW at each x-location to depict the portion of the JSW range represented by the radiographic measurement. Statistical analyses were completed using SAS version 9.2 (SAS Inc., Cary, NC).

Results

We recruited 20 participants (50% women; mean±SD age 66.8±5.7 years and BMI 29.6±5.0 kg/m^2). Out of the 40 knees imaged, 2 knees had motion artifact during the SCT image acquisition that precluded 3D JSW measurements and 3 knees had bone-on-bone contact, which interfered with segmentation. Of the 35 knees included, 40% were from female participants and mean±SD age and BMI were 66.9±5.5 years and 29.9±4.3 kg/m^2 respectively. The KL grades on the fixed-flexion PA radiographs of the included knees were KL0 (22.9%), KL1 (31.4%), KL2 (22.9%), and KL3 (22.9%).

The correlations between radiographic $JSW_{(x)}$ and 3D JSW were high, with an offset that was highly consistent in all knees at each x-location. Correlation coefficients and offsets between radiographic $JSW_{(x)}$ measurements and the 20^{th} and 60^{th} percentiles of anteroposterior JSW at each x-location are presented in Table 1. Although there was an offset between the measurements from the two modalities, there was consistency in the relationships between the radiographic $JSW_{(x)}$ values and distribution of JSW by SCT at each mediolateral location, with standard deviations for the mean differences between the modalities being ≤0.5mm at the most-medial 4 locations {x=0.150, 0.175, 0.200, 0.225}, and a greater offset between the measurements as well as greater variability in the offsets at locations closer to the tibial spines than the x=0.225 location.

Radiographic $JSW_{(x)}$ measurements were equivalent to the 3D JSW measured near the anterior and posterior extents of the concavity of the tibial plateau. Red circles in the example knee shown in Figure 5 depict the points of equivalent JSW measurements between radiographs and SCT at each x-location. This result was highly consistent across knees. As shown in Figures 5 and 6, the radiographic $JSW_{(x)}$ measurements were neither the maximum (near the 100^{th} percentile) nor the minimum (near the 0 percentile) JSW at each mediolateral

location. The slope of the relationship between radiographic $JSW_{(x)}$ (circles) and 3D JSW (shaded area) in Figure 6 reveals a consistent association for the 4 more medial locations (x=0.150–0.225), becoming less consistent at the locations closer to the tibial spines. At the most medial 4 locations, $JSW_{(x)}$ exceeded the minimal 3D JSW by a mean of 2.0mm and was equivalent to the 61st percentile of the anteroposterior JSW distribution at each respective x-location. For x=0.250 and 0.275 locations, the $JSW_{(x)}$ values exceeded the minimal 3D JSW by a mean of 2.6mm and were equivalent to the 65thand 70th percentiles of the anteroposterior JSW distribution, respectively. For the location closest to the tibial spines (x=0.300), the radiographic $JSW_{(x)}$ values exceeded the minimum JSW on SCT by a mean of 3.1 mm and was equivalent to the 79th percentile of the anteroposterior JSW distribution.

Discussion

Joint space width measurements on standardized standing flexed radiographs are a primary means of assessing tibiofemoral OA status. In this study, $JSW_{(x)}$ measurements from fixed flexion radiographs were found to differ from the minimum 3D JSW at each mediolateral x-location. The relationship between $JSW_{(x)}$ and 3D JSW from SCT was highly consistent between knees. The very high correlations between radiographic $JSW_{(x)}$ and the mid-range of 3D JSW values demonstrate that, while measurements of $JSW_{(x)}$ on radiographic projections overestimate the minimum JSW at each mediolateral x-location compared to SCT, there is a consistent offset, which is smaller at the more medial locations. Based on the correlations near 0.9, and small average paired differences between radiographic $JSW_{(x)}$ and 3D JSW on SCT at the x= 0.150 to 0.225 locations, this portion of the joint appears to be measured more consistently than portions closer to the tibial spines.

Potential reasons for the offset between the 2D and 3D JSW measurements include: 1) the varying degree of parallel alignment of the tibial plateau rims on radiographs, 2) the differences in the points that are selected for measurement using a silhouette (radiograph) in comparison with selecting nearest neighboring points on opposing 3D curved surfaces (due to sagittal tibiofemoral alignment), 3) areas within the tibia bone being selected on radiographs (the most radiopaque line), while the subchondral bone surface was clearly visualized on SCT, 4) a systematic magnification of anatomy on radiographs, 5) the minimum distance algorithm that was used for 3D JSW calculations determines the minimum distance between tibia and femur, while JSW_x measures the vertical distance depicted in Figure 2a.[20] With regard to radiographic alignment, the standard fixed-flexed standing radiograph protocol does not vary the x-ray beam angle or knee flexion in order to optimize the alignment of the tibial plateau rims for each patient, as do other protocols.[25; 26] A tibial intermargin distance of <1–1.5 mm is generally accepted as satisfactory parallel alignment.[27] Despite their differences in achieving parallel alignment, the construct validity has been found to be low[6] and not to significantly differ between fluoroscopically-guided and fixed-flexed radiographic techniques. The most likely reason for this relates to the inadequacy of 2D imaging for visualizing the bone edges at the narrowest point between the tibial plateau and femoral condyles. This point falls within a diffuse radiopaque region that results from a projection through a variety of 3D bony anatomy at the base of the tibia plateau, and therefore is not likely to correspond to the narrowest point identified from SCT. Furthermore, the location and thickness of this radiopaque region is highly dependent on

beam angle and degree of knee flexion. It likely does not correspond to the bone edge, but rather to points within the subchondral bone. In contrast, each of the bone edges is segmented on SCT, reducing ambiguity in distinguishing the joint margins.

The lower correlations between radiographic $JSW_{(x)}$ and JSW by SCT at locations closer to the tibial spines may also reflect the greater complexity of the overlapping anatomy in the coronal radiographic projection where the tibial plateau rims and floor converge near the tibial spines. This too could relate to the software that measures $JSW_{(x)}$ measuring points at varying depths within the subchondral bone, rather than the bone surface. The less consistent association of the radiographic $JSW_{(x)}$ measurement with the SCT measurement of JSW at the more central locations suggests that medial $JSW_{(x)}$ measurements from locations greater than approximately x=0.225 should be interpreted carefully. This finding is consistent with the report of Duryea et al that the x=0.225 location was superior to minimal JSW for knees with early OA,[28] and similar to the cartilage morphology at the central medial tibia. Likewise, we found that this location had the minimal difference in JSW comparing radiographic with SCT measurements.

Another possible reason for the measurement of radiographic $JSW_{(x)}$ exceeding that of 3D JSW on SCT may relate to the effect of sagittal tibiofemoral alignment (illustrated in Figure 7). In cases in which the curvatures of the bones closely approximate each other, measures of minimal JSW may be similar between modalities. However, in cases in which the femur is more anterior with respect to the tibia, the distance between the lines of maximal radiodensity on radiographs appear further apart than is found by a nearest-neighboring point measurement on the 3D surfaces (Figure 7).

In related studies using MRI as the reference standard, SCT imaging was found to be more sensitive and accurate for detection of osteophytes and subchondral cysts than conventional fixed-flexion radiography,[29] and 3D JSW on SCT was more closely correlated with WORMS cartilage morphology scores (*in press*). The results of the current study support a role for SCT in the evaluation of tibiofemoral OA. In addition, the inherent 3D nature of the SCT data makes patient-specific optimization of the joint-space viewing angle unnecessary. This should improve reliability and obviate the need for separate image acquisitions at multiple beam angles or use of fluoroscopic guidance, and it would also enable 3D evaluation of both the tibiofemoral and patellofemoral joints.

Imaging knees with OA using SCT may also have advantages over non-weight bearing MRI, due to imaging in a standing configuration. In KL grade 3 knees, Lyon-Schuss radiography has been reported to have greater sensitivity than quantitative MRI to change in articular cartilage thickness at 1 and 2 years. While the reason for this difference has not been fully elucidated, it could relate to the standing, weight-bearing configuration being more sensitive to softening of articular cartilage in knees with OA, whereas MRI may not detect such changes when acquired in a non-weight bearing position.[5]

When selecting an imaging modality, radiation dose is always a consideration. The effective dose is a calculated value that indicates the potential for long-term effects based on the absorbed dose, the relative harm level of the radiation and the sensitivity of the exposed

tissue to radiation. In comparison with an effective dose of 0.04-0.05mSv required for fixed-flexion knee radiographs (two lateral images and a bilateral PA view with potential need to repeat if beam angle requires correction), the effective radiation dose for SCT of bilateral knees in our study was 0.024mSv. The incident air kerma values at the entrance (skin) place for the SCT used in this study for two knees was 1.2 mGy, which compares favorably with (1) the 8–14 mGy skin entry dose (and 9 mGy central phantom dose) reported for another upright cone beam CT scanner for a single knee and (2) the skin entry dose reported for a traditional full-body multidetector CT for one or two knees (27–40 mGy).[30] Therefore, the greater accuracy and wealth of information available in the 3D SCT imaging dataset were achieved without a clinically significant increase in radiation dose.

While this study extended knowledge regarding the correlation and offset between radiographic $JSW_{(x)}$ and 3D JSW measurements on SCT, there were several limitations. The fixed-flexed radiographs and SCT were not completed simultaneously, so differences in the knee flexion angle cannot be ruled out with certainty. As the cone beam SCT natively acquires the equivalent of 360 radiographs, future research could compare the fixed-flexed PA radiographic view to the 3D JSW. This was not done in this study, as the aim was to better characterize a widely used fixed-flexed radiographic protocol for generalization of study findings.

Another limitation was the need for extensive human input to obtain accurate segmentations of the bone edges, due to the differences in bone density within areas of the joint (e.g. medial and lateral limits of the femoral condyles) and also between joints. While this was not a scientific limitation, an ongoing need for this degree of human input could limit the usefulness of 3D JSW measurements on SCT. However, through completion of this and additional follow-up studies, the degree of manual input subsequently has been reduced. An additional potential limitation was the difference in imaging resolution. In comparison with radiographs (0.2mm pixels), a 0.37mm voxel was chosen for 3D imaging of knees with SCT in order to balance resolution performance (image quality, dynamic range, contrast etc.) with scan time and radiation exposure. The resolution is a function of the magnification, pixel size, and available system resources. At the time of this study, the SCT had an SID of 760mm, and an SAD of 535mm, yielding a nominal magnification factor of 1.42. This limited meaningful voxel size when reconstructed to 0.388/1.42 = 0.27mm. The field of view forced a memory limit that prevented higher resolution than 0.37mm. However, that memory limitation has since been alleviated, allowing reconstruction with 0.3 mm voxel size, with a visible improvement in spatial resolution.

This study was designed to compare only JSW measurements that are possible with radiographs with JSW measurements by SCT. SCT visualizes meniscal extrusion on non-contrast scans, such as the ones used in this study. In addition, cartilage thickness and cartilage loss can be measured on SCT arthrography. As femoral cartilage loss, tibial cartilage loss and meniscus height loss cannot be distinguished on radiographs, a comparison could not be made in the current study. Another limitation of the current study was that a static fixed-flexed posture was used to compare with the accepted radiographic protocol, but this degree of flexion is not the only angle at which the knee is loaded during

functional activities. This limitation could be overcome by measuring JSW during dynamic loading or at multiple flexion angles.

Further research will need to characterize the responsiveness of SCT imaging to changes over time. This current study assessed correlations between radiographic and 3D JSW by SCT cross-sectionally, providing justification for a longitudinal study to measure responsiveness to narrowing of JSW over time, a more clinically meaningful measurement of the potential advantages of SCT. If the responsiveness to progression of joint space narrowing were found to be greater than that for radiographs, then it would represent an important advantage of SCT over radiography. The sensitivity of joint space narrowing on AP radiographs for detecting cartilage loss has been reported to be 46%.[31] Use of SCT has high potential to improve the diagnostic performance due to the abilities to view individual coronal and sagittal slices as well as to visualize the meniscus.

Another focus for future research is characterization of the weight-bearing patellofemoral joint. The capacity to clearly image the joint while standing, and to obtain a more functional relationship of the patella to the femoral trochlea than a non-weightbearing view, could enhance understanding of joint anatomy and pathology and if responsiveness to joint space narrowing were high, then clinical trials and clinical care could be significantly enhanced.

In conclusion, for the knees studied, 3D JSW values on SCT correlate highly with radiographic $JSW_{(x)}$, with a consistent offset at the more medial x-locations (x=0.15–0.225). The offset of radiographic $JSW_{(x)}$ relative to 3D JSW is likely due to overlapping anatomy obscuring portions of the joint on radiographs.

Acknowledgments

The authors thank the participants of the Multicenter Osteoarthritis (MOST) Study who volunteered their time for this study, as well as Tricia Feldick and Natalie Glass for essential assistance with recruitment and data collection. Research reported in this manuscript was supported by the National Institute of Arthritis and Musculoskeletal and Skin Diseases of the National Institutes of Health under award number P50AR055533, as well as by the the National Institute on Aging: *Boston University (David Felson, MD - AG18820); The University of Iowa (James Torner, PhD - AG18832); University of California San Francisco (Michael Nevitt, PhD - AG19069).* The content is solely the responsibility of the authors and does not necessarily represent the official views of the National Institutes of Health. The SCT unit was lent by CurveBeam, LLC to Dr. Segal's lab without stipulations regarding its use.

References

1. Felson DT. An update on the pathogenesis and epidemiology of osteoarthritis. Radiologic clinics of North America. 2004; 42:1–9. v. [PubMed: 15049520]
2. Brandt KD, Fife RS, Braunstein EM, et al. Radiographic grading of the severity of knee osteoarthritis: relation of the Kellgren and Lawrence grade to a grade based on joint space narrowing, and correlation with arthroscopic evidence of articular cartilage degeneration. Arthritis Rheum. 1991; 34:1381–1386. [PubMed: 1953815]
3. Guermazi A, Niu J, Hayashi D, et al. Prevalence of abnormalities in knees detected by MRI in adults without knee osteoarthritis: population based observational study (Framingham Osteoarthritis Study). BMJ. 2012; 345:e5339. [PubMed: 22932918]
4. Guermazi A, Hayashi D, Roemer FW, et al. Osteoarthritis: a review of strengths and weaknesses of different imaging options. Rheum Dis Clin North Am. 2013; 39:567–591. [PubMed: 23719076]

5. Guermazi A, Roemer FW, Felson DT, et al. Motion for debate: osteoarthritis clinical trials have not identified efficacious therapies because traditional imaging outcome measures are inadequate. Arthritis Rheum. 2013; 65:2748–2758. [PubMed: 23861096]
6. Javaid MK, Lynch JA, Tolstykh I, et al. Pre-radiographic MRI findings are associated with onset of knee symptoms: the most study. Osteoarthritis Cartilage. 2010; 18:323–328. [PubMed: 19919856]
7. FDA. , editor. Federal Register. Clinical Development Programs for Human Drugs, Biological Products, and Medical Devices for the Treatment and Prevention of Osteoarthritis; p. 126August 14, 2007. DOCKET NO. 1998D - 0077 (FORMERLY 98D - 0077)
8. Amin S, LaValley MP, Guermazi A, et al. The relationship between cartilage loss on magnetic resonance imaging and radiographic progression in men and women with knee osteoarthritis. Arthritis Rheum. 2005; 52:3152–3159. [PubMed: 16200595]
9. Felson D, Niu J, Sack B, et al. Progression of osteoarthritis as a state of inertia. Ann Rheum Dis. 2013; 72:924–929. [PubMed: 22753401]
10. FDA. , editor. Federal Register. Clinical Development Programs for Human Drugs, Biological Products, and Medical Devices for the Treatment and Prevention of Osteoarthritis; p. 100August 14, 2007. DOCKET NO. 1998D - 0077 (FORMERLY 98D - 0077)
11. Abramson SB, Berenbaum F, Hochberg MC, et al. Introduction to OARSI FDA initiative OAC special edition. Osteoarthritis Cartilage. 2011; 19:475–477. [PubMed: 21396473]
12. Duryea J, Jiang Y, Zakharevich M, et al. Neural network based algorithm to quantify joint space width in joints of the hand for arthritis assessment. Med Phys. 2000; 27:1185–1194. [PubMed: 10841426]
13. Kalinosky B, Sabol JM, Piacsek K, et al. Quantifying the tibiofemoral joint space using x-ray tomosynthesis. Med Phys. 2011; 38:6672–6682. [PubMed: 22149849]
14. Segal NA, Anderson DD, Iyer KS, et al. Baseline articular contact stress levels predict incident symptomatic knee osteoarthritis development in the MOST cohort. J Orthop Res. 2009; 27:1562–1568. [PubMed: 19533741]
15. Segal NA, Kern AM, Anderson DD, et al. Elevated tibiofemoral articular contact stress predicts risk for bone marrow lesions and cartilage damage at 30 months. Osteoarthritis Cartilage. 2012; 20:1120–1126. [PubMed: 22698440]
16. Segal NA, Nevitt MC, Gross KD, et al. The Multicenter Osteoarthritis Study: opportunities for rehabilitation research. PM R. 2013; 5:647–654. [PubMed: 23953013]
17. Kellgren JH, Lawrence JS. Radiological assessment of osteo-arthrosis. Ann Rheum Dis. 1957; 16:494–502. [PubMed: 13498604]
18. Felson DT, Nevitt MC, Yang M, et al. A new approach yields high rates of radiographic progression in knee osteoarthritis. J Rheumatol. 2008; 35:2047–2054. [PubMed: 18793000]
19. Kothari M, Guermazi A, von Ingersleben G, et al. Fixed-flexion radiography of the knee provides reproducible joint space width measurements in osteoarthritis. Eur Radiol. 2004; 14:1568–1573. [PubMed: 15150666]
20. Duryea J, Li J, Peterfy CG, et al. Trainable rule-based algorithm for the measurement of joint space width in digital radiographic images of the knee. Med Phys. 2000; 27:580–591. [PubMed: 10757609]
21. Duryea J, Zaim S, Genant HK. New radiographic-based surrogate outcome measures for osteoarthritis of the knee. Osteoarthritis Cartilage. 2003; 11:102–110. [PubMed: 12554126]
22. Duryea J, Neumann G, Niu J, et al. Comparison of radiographic joint space width with magnetic resonance imaging cartilage morphometry: analysis of longitudinal data from the Osteoarthritis Initiative. Arthritis Care Res (Hoboken). 2010; 62:932–937. [PubMed: 20589702]
23. Li W, Anderson DD, Goldsworthy JK, et al. Patient-specific finite element analysis of chronic contact stress exposure after intraarticular fracture of the tibial plafond. J Orthop Res. 2008; 26:1039–1045. [PubMed: 18404662]
24. Anderson DD, Goldsworthy JK, Li W, et al. Physical validation of a patient-specific contact finite element model of the ankle. J Biomech. 2007; 40:1662–1669. [PubMed: 17433333]
25. Buckland-Wright JC, Wolfe F, Ward RJ, et al. Substantial superiority of semiflexed (MTP) views in knee osteoarthritis: a comparative radiographic study, without fluoroscopy, of standing

extended, semiflexed (MTP), and schuss views. J Rheumatol. 1999; 26:2664–2674. [PubMed: 10606380]

26. Piperno M, Hellio Le Graverand MP, Conrozier T, et al. Quantitative evaluation of joint space width in femorotibial osteoarthritis: comparison of three radiographic views. Osteoarthritis Cartilage. 1998; 6:252–259. [PubMed: 9876394]
27. Hellio Le Graverand MP, Mazzuca S, Duryea J, et al. Radiographic grading and measurement of joint space width in osteoarthritis. Rheum Dis Clin North Am. 2009; 35:485–502. [PubMed: 19931800]
28. Neumann G, Hunter D, Nevitt M, et al. Location specific radiographic joint space width for osteoarthritis progression. Osteoarthritis Cartilage. 2009; 17:761–765. [PubMed: 19073368]
29. Segal NA, Nevitt MC, Lynch JA, et al. Diagnostic performance of 3D standing CT imaging for detection of knee osteoarthritis features. The Physician and sportsmedicine. 2015; 43:213–220. [PubMed: 26313455]
30. Carrino JA, Al Muhit A, Zbijewski W, et al. Dedicated cone-beam CT system for extremity imaging. Radiology. 2014; 270:816–824. [PubMed: 24475803]
31. Kijowski R, Blankenbaker DG, Stanton PT, et al. Radiographic findings of osteoarthritis versus arthroscopic findings of articular cartilage degeneration in the tibiofemoral joint. Radiology. 2006; 239:818–824. [PubMed: 16641340]

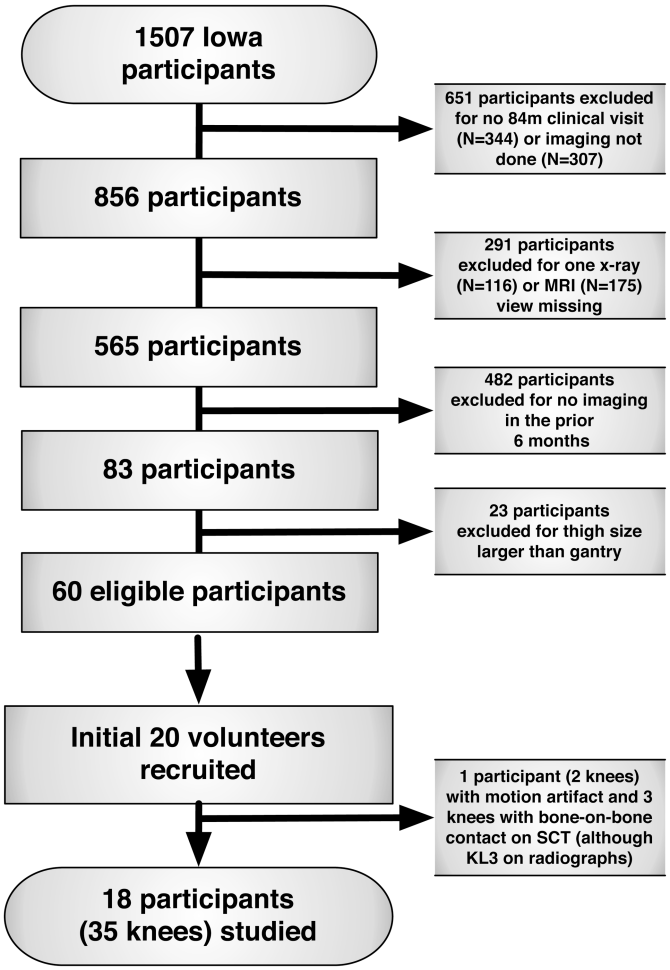

Figure 1.
Flowchart for inclusion of participants

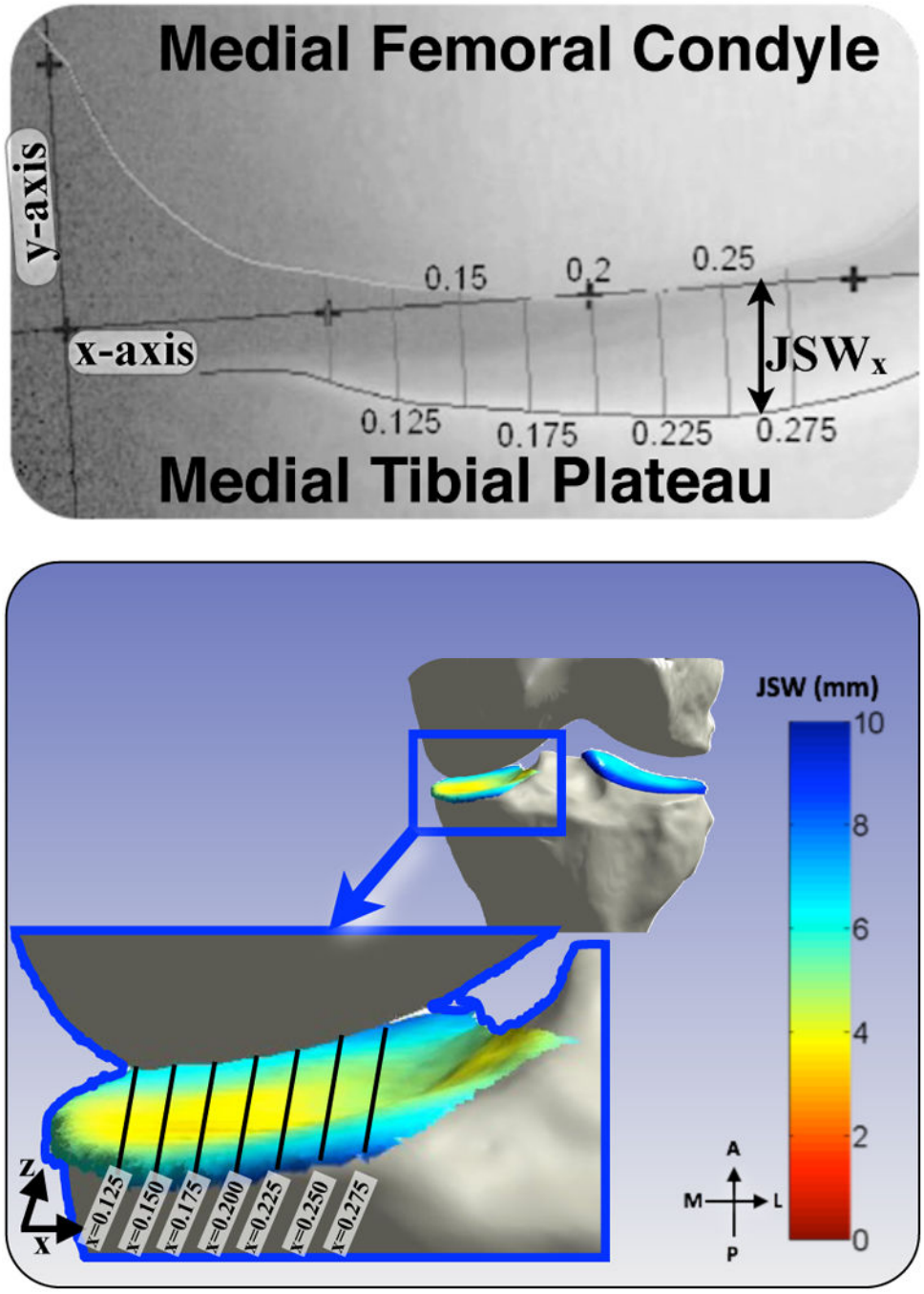

Figure 2.

(a) Radiographic JSW(x) is measured at each x-location, shown here as lines connecting the delineated tibial plateau to nearest points on the projection of the femoral margin. (b) 3D JSW measured from SCT reflects the proximity of the distal femur subchondral bone to its nearest neighbor on the proximal tibia. The distribution can be sampled at fixed x-locations for comparison with the radiographic JSW(x).

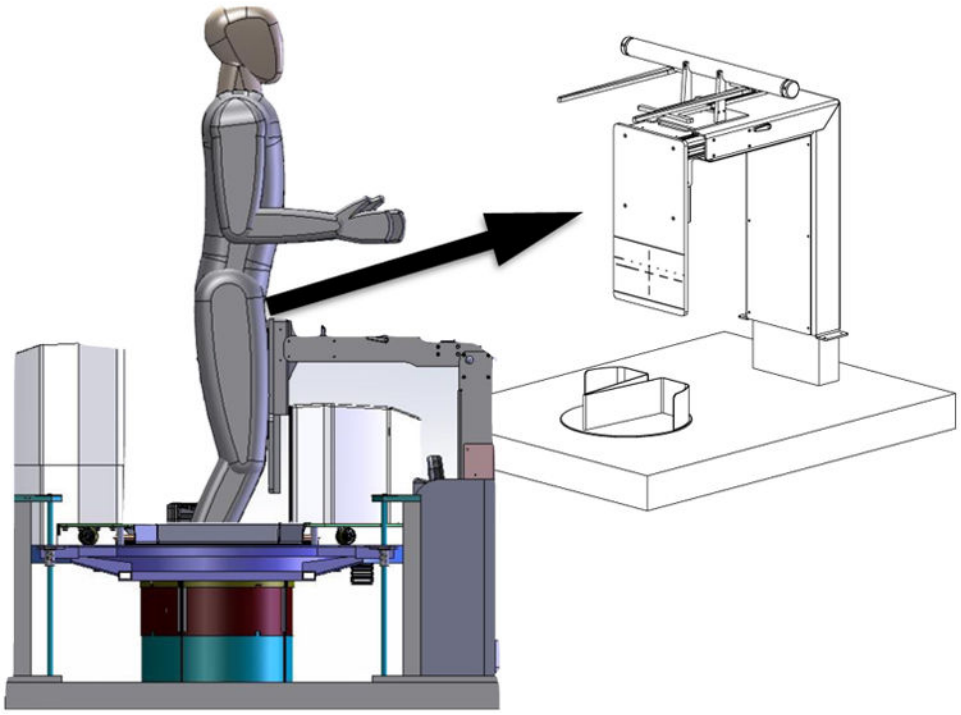

Figure 3.
Radiolucent Fixed Flexion Frame in SCT Scanner: (Left) Illustration of subject in the SCT. (Right) Detail of positioning frame for the pelvis, thighs and feet that allows reproducible imaging of the knee.

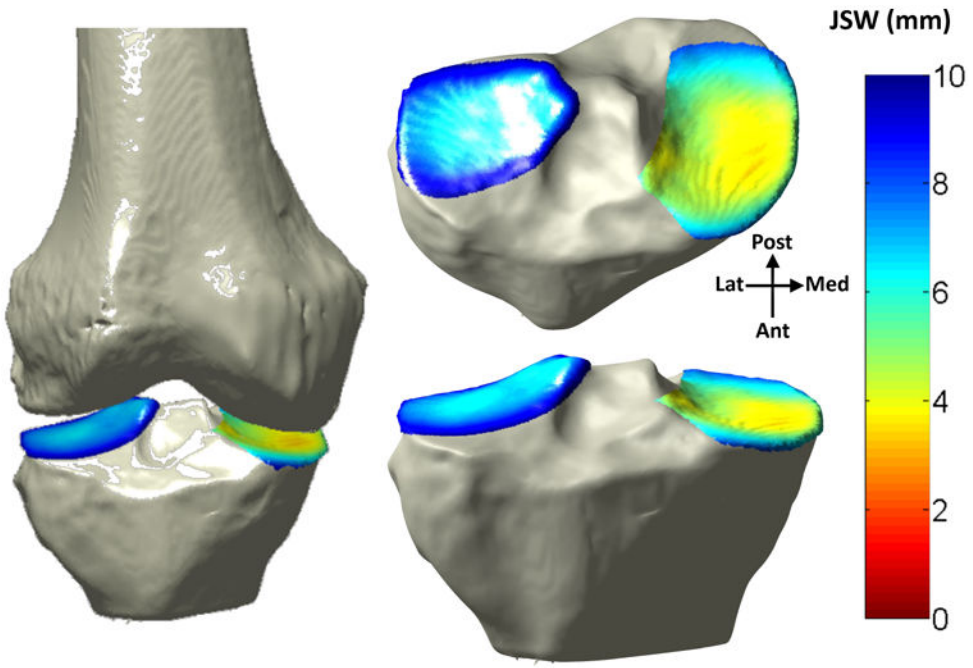

Figure 4.

The tibiofemoral 3D JSW mapping is depicted as a color map on the subchondral surface of the proximal tibia.

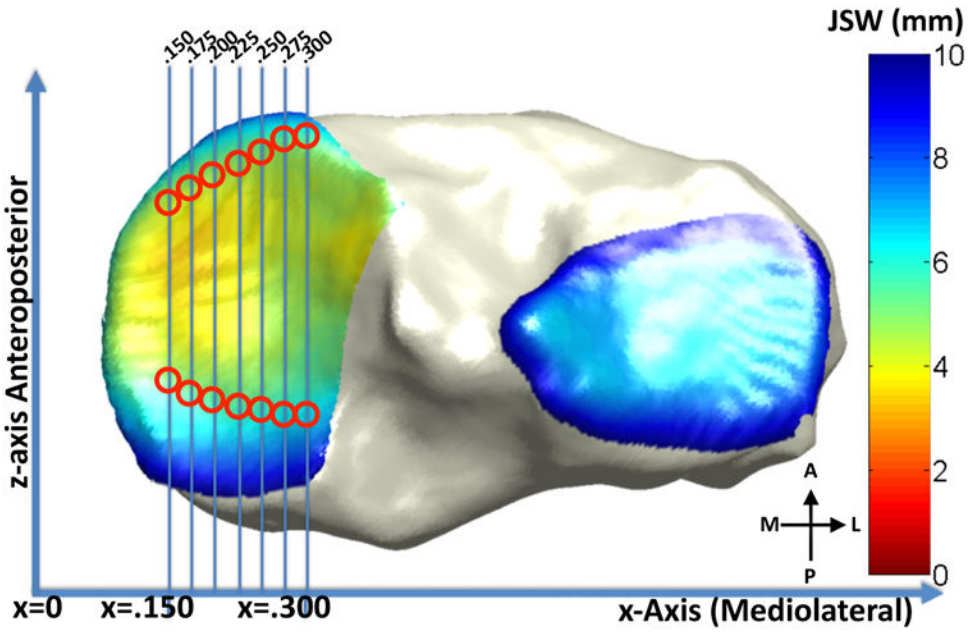

Figure 5.

The anatomic locations of approximate equivalency between radiographic JSW(x) and the 3D JSW measurements are shown at fixed x-locations across the medial compartment of the proximal tibia.

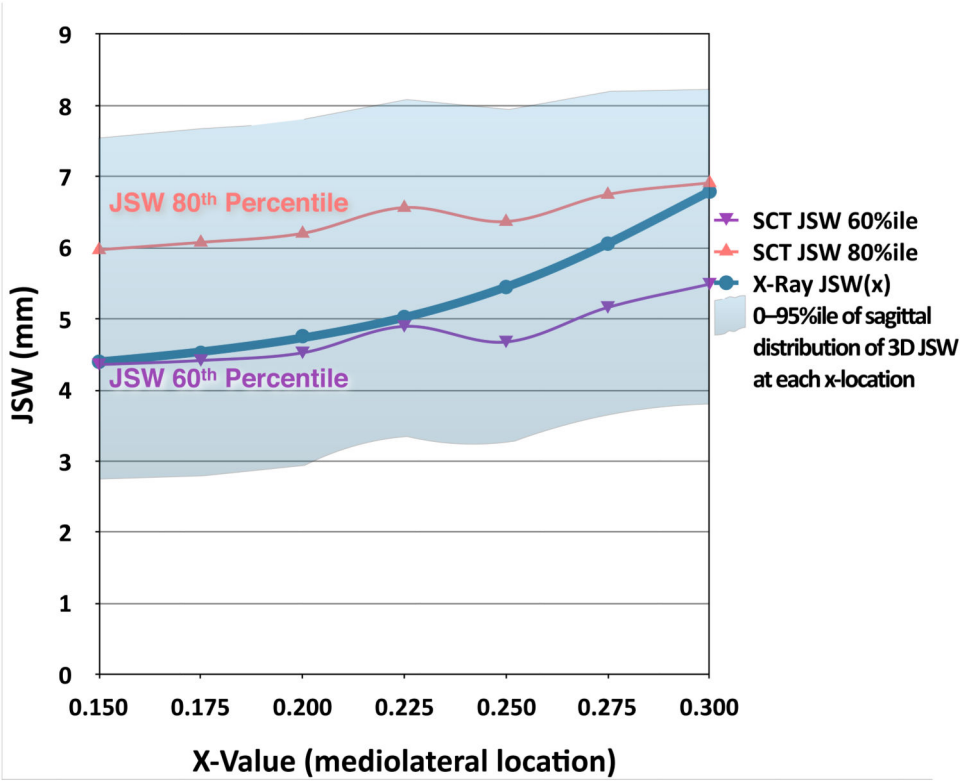

Figure 6.

The SCT JSW values were highly correlated with the JSW(x) values. There was close agreement between the 61th percentile of the anteroposterior distribution of 3D JSW on SCT and the corresponding single value of $JSW_{(x)}$ at the 4 more medial x-locations, with less close agreement at the more lateral locations.

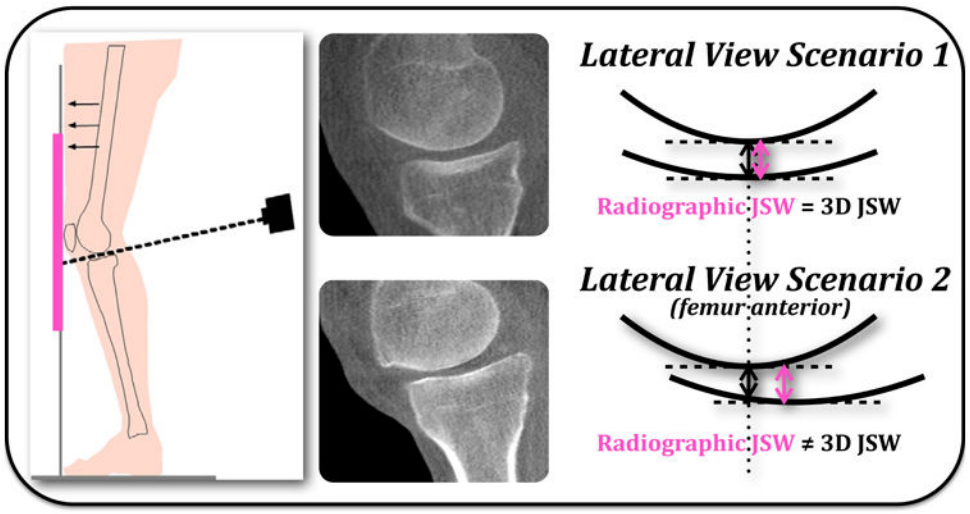

Figure 7.
This graphic depicts one possible scenario explaining differences in the minimal JSW values measured on radiographic projections versus those measured on 3D SCT.

Table 1

Comparisons between the JSW(x) values and 20th and 60th percentile values of the 3D JSW distribution along a sagittal plane at a given x-location

x-location	0.150	0.175	0.200	0.225	0.250	0.275	0.300
Correlation between $JSW_{(x)}$ and the 20%ileof 3D JSW	0.97 (0.94, 0.99)	0.96 (0.92, 0.99)	0.95 (0.89, 0.98)	0.93 (0.86, 0.97)	0.93 (0.87, 0.97)	0.91 (0.84, 0.95)	0.91 (0.82, 0.96)
Paired difference between JSWx at 20^{th} percentile of 3D JSW(mm); mean (95%CI)	1.5 (0.9, 2.1) *	1.5 (0.9, 2.2) *	1.6 (0.9, 2.4) *	1.4 (0.4, 2.4) *	2.1 (1.2, 3.0) *	2.1 (0.9, 3.3) *	2.6 (1.2, 4.0) *
Correlation between JSW(x) and the 60th percentile of 3D JSW	0.80 (0.60, 0.95)	0.88 (0.73, 0.96)	0.90 (0.78, 0.96)	0.91 (0.85, 0.95)	0.89 (0.80, 0.94)	0.93 (0.87, 0.97)	0.94 (0.88, 0.98)
Paired difference between JSWx at 60^{th} percentile of 3D JSW(mm); mean (95%CI)	0.0 (-1.9, 1.8)	0.1 (-1.3, 1.5)	0.2 (-1.0, 1.4)	0.2 (-0.,9, 1.3)	0.8 (-0.5, 2.0)	1.0 (-0.1, 2.1)	1.4 (0.2, 2.6) *

* For paired differences between modalities, p<0.0001